



HAL
open science

Depletion induced vesicle-to-micelle transition from self-assembled rod-coil diblock copolymers with spherical magnetic nanoparticles

Willy Agut, Daniel Taton, Annie Brûlet, Olivier Sandre, Sébastien Lecommandoux

► To cite this version:

Willy Agut, Daniel Taton, Annie Brûlet, Olivier Sandre, Sébastien Lecommandoux. Depletion induced vesicle-to-micelle transition from self-assembled rod-coil diblock copolymers with spherical magnetic nanoparticles. *Soft Matter*, 2011, 7 (20), pp.9744-9750. 10.1039/c1sm05638g . hal-00668996

HAL Id: hal-00668996

<https://hal.science/hal-00668996v1>

Submitted on 3 Nov 2018

HAL is a multi-disciplinary open access archive for the deposit and dissemination of scientific research documents, whether they are published or not. The documents may come from teaching and research institutions in France or abroad, or from public or private research centers.

L'archive ouverte pluridisciplinaire **HAL**, est destinée au dépôt et à la diffusion de documents scientifiques de niveau recherche, publiés ou non, émanant des établissements d'enseignement et de recherche français ou étrangers, des laboratoires publics ou privés.

Depletion Induced Vesicle-to-Micelle Transition from Self-Assembled Rod-Coil Diblock Copolymers with Spherical Magnetic Nanoparticles

Willy Agut,^{a,b} Daniel Taton,^{a,b} Annie Brûlet,^{c,d} Olivier Sandre,^{*a,b} and Sébastien Lecommandoux^{*a,b}

Received 10th April 2011, Accepted 1st June 2011

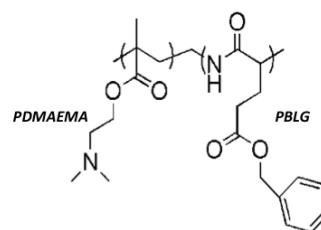
DOI: 10.1039/C1SM05638G

This article describes the structural transition undergone by a vesicle forming diblock copolymer made of a hydrophobic poly(γ -benzyl-L-glutamate) sequence with helical secondary structure and of a hydrophilic poly[2-(dimethylamino)ethyl methacrylate] block when inserting hydrophobic iron oxide nanoparticles to impart magnetic properties in addition to pH- and temperature-responsiveness. Dispersed within the hydrophobic rod-like polymer domains, the quasi-spherical particles experience depletion attraction, leading to microphase separation and finally to transition from vesicles to hybrid core-shell micelles. Such combination of self-assembly with excluded-volume effects, also present in living systems and giving rise to such a large structural diversity and functionality, can be integrated in materials science towards the design of original nanostructures.

1. Introduction

Most of the biological materials are soft with a structure and function resulting from self-assembly of multiple components differing by their molecular weight, size, shape, amphiphilicity and elasticity. In first approximation, such complex systems can be analysed using soft matter physics approaches.¹ Among others, rod-like molecules such as actin filaments or DNA are important in many biological systems where steric effects, due to the high local concentration resulting from compartmentalization, are known as “macromolecular crowding”.² Because osmotic forces are not restricted to particular components and length scales, the underlying principle of depletion interaction that is well-known in macromolecular science and physics is also applicable to biological systems. While the understanding of depletion forces in bi-modal spherical colloids³ and colloid-polymer systems⁴ is advanced, less is known when colloidal rods are used as depletion agent.

Amphiphilic block copolymers are known to self-assemble into well-defined structures depending on their hydrophilic-to-hydrophobic weight ratio. In particular, a hydrophilic fraction in a range of 30 – 40% leads to the formation of vesicles referred to as polymersomes.⁵ Recently, we reported the synthesis of block copolymers featuring, on the one hand, a rigid poly(γ -benzyl-L-glutamate) (PBLG) polypeptide sequence exhibiting α -helical secondary structure and, on the other hand, a hydrophilic block poly[2-(dimethylamino)ethyl methacrylate] (PDMAEMA), which displays a dual responsiveness to both pH ($pK_a=7.7$) and temperature ($LCST=39^\circ C$).⁶ More generally, the propensity of amphiphilic copolymers based on PBLG blocks to self-assemble into polymersomes is well-documented.⁷ The formation of polymer vesicles is indeed facilitated by the two-dimensional stacking of rod-like PBLG helices into planar membranes.



Scheme 1 Amphiphilic diblock copolymer made of a hydrophilic thermosensitive block (PDMAEMA) and a hydrophobic rod-like polypeptide block (PBLG)

Ultra-small superparamagnetic iron oxide particles (USPIO) are individual nanoparticles made of either γ -Fe₂O₃ or Fe₃O₄ used as negative contrast-enhancing agents in magnetic resonance imaging under the brand names of Sinerem or Ferumoxtran. To achieve improved properties (proton relaxivity in MRI, biodistribution, specific absorption rate in radio-frequency hyperthermia...), SPIO particles which can be viewed as controlled clusters of USPIOs of size typically below 200 nm are generally preferred to USPIOs.⁸ Relatively well-controlled clusters are obtained by using strong adsorbing hydrophilic homopolymers such as Dextran,⁹ or with copolymers forming micelles,¹⁰ coacervates¹¹ or microgels.¹² Formation of polymersomes confining USPIOs between the leaflets of their hydrophobic membrane was reported in the case of a few amphiphilic copolymers, namely poly(butadiene)-*b*-poly(L-glutamic acid) (PB-*b*-PGA),¹³ poly(isoprene)-*b*-poly(ethylene oxide) (PI-*b*-PEO),¹⁴ poly(styrene)-*b*-poly(acrylic acid) (PS-*b*-PAA),¹⁵ and poly(trimethylene carbonate)-*b*-poly(L-glutamic acid) (PTMC-*b*-PGA).¹⁶

In this paper, we report on the self-assembly of amphiphilic block copolymers comprising a rod-like segment in the presence of quasi-spherical nanoparticles. We aim at demonstrating that

depletion forces can strongly influence the self-assembly properties in such binary systems and can be presented as an original trigger to drive the equilibrium structures.

2. Experimental

A. Synthesis and coupling of polymer blocks

As described in a previous report,¹⁷ the poly(γ -benzyl-L-glutamate)-*b*-poly[2-(dimethylamino)ethyl methacrylate] (PBLG-*b*-PDMAEMA) block copolymer was synthesized by the Huisgen's 1,3-dipolar cycloaddition ("click chemistry") from the PBLG and PDMAEMA homopolymers containing azide and alkyne antagonist functionalities.

B. Synthesis and coating of the magnetic nanoparticles

USPIOs made of γ -Fe₂O₃ iron oxide were synthesized by alkaline co-precipitation of iron salts in water.¹⁸ Using a size sorting procedure,¹⁹ the distribution of diameters was narrowed so as to be described by a Log-normal distribution of median value $d_0=6.3$ nm and width $\sigma=0.22$ as measured by magnetometry (Fig. S1 in SI). Then the USPIOs were coated by an anionic surfactants mixture of alkylethoxyphenol mono- and diesters of phosphoric acid (Beycostat NB09, CECA, Arkema group),²⁰ enabling a perfect dispersed state in dichloromethane ($R_H=9.4$ nm).

C. Self-assembly processes

i. Direct dissolution

The hydrophilic-lipophilic balance allowed a direct dissolution of the copolymer (1 g/L) by simple stirring for 48h in distilled water (pH 6.5) at 25°C or 105°C under reflux.²¹

ii. Solvent injection or "nano-precipitation"

Unlike with molecular surfactants readily forming mesophases at thermodynamic equilibrium when poured into water, the self-assembly of amphiphilic copolymers can be hampered by kinetic issues when using glassy or semi-crystalline blocks such as in the PDMAEMA-*b*-PBLG used here. In that case, a solvent injection (displacement) method is generally preferred to direct dissolution. An intermediate solvent is used to solubilise the copolymer while being miscible with water.²² By tuning the mixing conditions, the inter-diffusion kinetics between the two solvents is controlled, which maintains the chains in a dynamical state all along the self-assembly process, improving the control of the sizes of the resulting nanoparticles. The PDMAEMA-*b*-PBLG copolymer was dissolved at 10 g/L in THF or in DMSO. Then an aqueous solution buffered at pH 6.5 was added at constant flow rate (0.1 mL/min with a syringe pump) under vigorous stirring (400 rpm with a magnetic bar) until reaching a volumetric ratio 9/1 of water to solvent and a copolymer concentration of 1 g/L. The organic solvent was removed from the suspension by extensive dialysis in water (pH 6.5), except for the samples used in SANS experiments to avoid the use of a large volume of D₂O. For the preparation of hybrid objects, a dispersion of USPIOs at 95 g/L in CH₂Cl₂ was added to the organic solution in DMSO at a feed weight ratio of 10 or 20 wt. % relatively to the copolymer (0.1 or 0.2 g/L). After rapid evaporation of CH₂Cl₂, the nanoprecipitation was conducted as described before.

D. Methods

Size exclusion chromatography (SEC) was used to determine molar masses (calibrated with linear PS standards) and their dispersities in DMF + LiBr (1g/L) at 60°C (0.8 mL/min) with a Waters system (Alliance GPCV2000) equipped with three TSK columns (7.8×30 cm, 5 μ m of respective pores' sizes 250, 1500 and 10000 Å) and a differential refractometer (Jasco, RI-1530).

NMR ¹H and ¹³C spectra were done on a 400 MHz Bruker AC400 spectrometer.

Differential Scanning Calorimetry (DSC) curves were acquired on a Q100 DSC setup (TA Inst.) under helium flow. Temperature ramps between -50°C and 150°C were done at 10°C/min.

Transmission electronic microscopy (TEM) micrographs were obtained on a Hitachi H7650 microscope operating at 80kV and grabbed with a Gatan Orius 11 Mpixels camera. Samples were prepared by spraying aqueous solutions at 1mg/mL with a home-made nitrogen nebulizer on carbon films of 400 mesh grids and then dried under air at room temperature.

Dynamical Light Scattering was performed using an ALV Laser goniometer, which consisted of a 35 mW HeNe linear polarized laser with a wavelength of 632.8 nm and an ALV-5000/EPP Multiple Tau Digital correlator with 125 ns initial sampling time. DLS measurements were either mono-angle (90°) or multi-angle (ranging from 50° to 130°). Aliquots of samples (1 mL in a 10 mm diameter cylindrical glass cell) were immersed in a filtered toluene bath regulated at 25 °C. The data were acquired with the ALV-Correlator Control software with a counting time between 60 and 300 s depending on the angle. The intensity correlograms were treated by the CONTIN fit to obtain the distribution of the correlation times and by the cumulants fit to yield the z -average hydrodynamic radius (R_H) through Stokes-Einstein's formula and the polydispersity index (PDI) from the ratio of the 2nd order cumulant divided by the square of the 1st order one.

Small Angle Neutron Scattering measurements were performed on the PACE spectrometer of the Laboratoire Léon Brillouin (CEA-Saclay, France) equipped with an isotropic BF₃ detector made of 30 concentric rings of 1 cm width each. We used two configurations: the first one with a sample-to-detector distance of $D=4.57$ m and a neutron wavelength of $\lambda=17$ Å to cover a q range of $3.2\times 10^{-3} - 2.6\times 10^{-2}$ Å⁻¹; the second one with $D=2.87$ m and $\lambda=6$ Å to cover a q range of $1.1\times 10^{-2} - 0.1$ Å⁻¹.

The neutron scattering-length density (SLD) of the hydrophilic blocks $\rho^{\text{PDMAEMA}}=8\times 10^9$ cm⁻² is comparable to the magnetic SLD of the USPIOs $\rho^{\text{mag Fe}_2\text{O}_3}=9\times 10^9$ cm⁻². Both of them are far away from the nuclear SLDs of the USPIOs $\rho^{\text{nuc Fe}_2\text{O}_3}=7\times 10^{10}$ cm⁻² and of the hydrophobic blocks of the copolymer $\rho^{\text{PBLG}}=2.3\times 10^{10}$ cm⁻². In pure H₂O ($\rho^{\text{H}_2\text{O}}=-0.56\times 10^9$ cm⁻²), one observes mainly the nuclear scattering of USPIOs ($\Delta\rho^{\text{Fe}_2\text{O}_3}=7.5\times 10^{10}$ cm⁻²) but also in a reduced way (*i.e.* 7 times lower contrast value $\Delta\rho^2$) of the hydrophobic core of the copolymer ($\Delta\rho^{\text{PBLG}}=2.8\times 10^{10}$ cm⁻²). The solvent of nanoprecipitated samples was a 9:1 mixture of D₂O and deuterated DMSO ($\rho^{\text{D}_2\text{O/DMSO-d}_6}=6.2\times 10^{10}$ cm⁻²) leading to a low contrast $\Delta\rho^{\text{Fe}_2\text{O}_3}=8.1\times 10^9$ cm⁻² with γ -Fe₂O₃ and high contrasts with both the polymer blocks $\Delta\rho^{\text{PBLG}}=3.9\times 10^{10}$ cm⁻² and $\Delta\rho^{\text{PDMAEMA}}=5.4\times 10^{10}$. To minimize the incoherent scattering, the SANS measurements were done in quartz cuvettes of thickness respectively 5 mm for D₂O/DMSO-d₆ and 1 mm for H₂O. All the scattered intensity curves were normalized by the incoherent signal delivered by a 1 mm gap water sample in order to account

for the efficiency of the detector cells and the incoherent backgrounds of the solvents were subtracted. Absolute values of the scattering intensity $I(q)$ in cm^{-1} were obtained from the direct determination of the number of neutrons in the incident beam and the detector cell solid angle.²³

3. Results

A. Characterisation of the copolymer

Table 1 Molecular characteristics of the PDMAEMA-*b*-PBLG copolymer

Sample	$M_{n,\text{PDMAEMA}}^a$	$M_{n,\text{PBLG}}^a$	$M_{n,\text{copolymer}}^a$	PDI ^a
PDMAEMA ₈₅ - <i>b</i> -PBLG ₄₁	13300	9000	22300	1.17

^a Determined by SEC in DMF at 60 °C in the presence of LiBr; calibration with polystyrene standards.

The characterisation of the copolymer by NMR and SEC reported in Table 1 led to a hydrophobic weight fraction $f_{\text{PBLG}}=40\%$. The glass transition temperatures of both homopolymers and of the copolymer assessed by DSC all ranged between 10 and 20°C (Fig. S2 in SI). Moreover, a melting transition (from crystal to liquid-crystal state) was detected around 100°C and ascribed to the irreversible conformational change from 7/2 to 18/5 helices of the PBLG helices.²⁴ These characteristic transition temperatures in bulk are important to tune the self-assembling properties in solution.

B. Pure block copolymer self-assembly

i. Direct dissolution

Table 2 Hydrodynamic radii (R_H) and polydispersity indexes (PDI) obtained by direct dissolution of PDMAEMA₈₅-*b*-PBLG₄₁ at 1g/L at several values of temperature and pH.

T^a	T^b	pH ^a	pH ^b	R_H	PDI
25°C	25°C	6.5	6.5	107	0.43
105°C	25°C	6.5	6.5	58	0.44
105°C	25°C	2.5	2.5	46	0.19
105°C	25°C	2.5	7.2	46	0.31
105°C	25°C	2.5	11.4	43	0.43

^a during dissolution; ^b during DLS measurement.

The hydrodynamic radius R_H of the objects formed by direct dissolution (Fig. 1 and Table 2) in water at pH 6.5 decreased from 107 nm at 25°C (just above glass transition of the copolymer) to 58 nm at 105°C (just above the melting temperature of PBLG). However, size distributions remained very large (PDI=0.43). An attempt was made to narrow the size distribution by saturating the positive charge of PDMAEMA during dissolution at pH 2.5 well below the $\text{pK}_a=7.7$ of the ammonium moiety, promoting electrostatic repulsions between the objects. This enabled to decrease both R_H and PDI down to 46 nm and 0.19 respectively. However, the PDI returned to high values by progressively rising up the pH, presumably due to the apparition of a slight portion of aggregates. As a result, due to the intrinsic rigidity of PBLG and its crystalline behaviour below 100°C, the direct self-assembly of the copolymer leads to unstable and poorly defined structures.

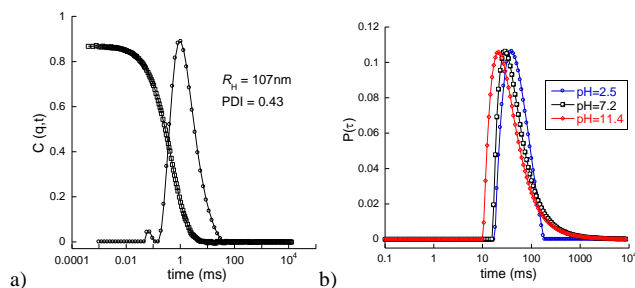


Fig. 1 DLS correlograms at a scattering angle of 90° and distributions of the correlation times $P(\tau)$ for PDMAEMA₈₅-*b*-PBLG₄₁ directly dispersed in water at 25°C and pH 6.5 (a) and at 105°C and varying pH (b).

ii. Solvent injection or “nano-precipitation”

In order to better control the self-assembly process, we implemented the nanoprecipitation method using two different intermediate solvents.

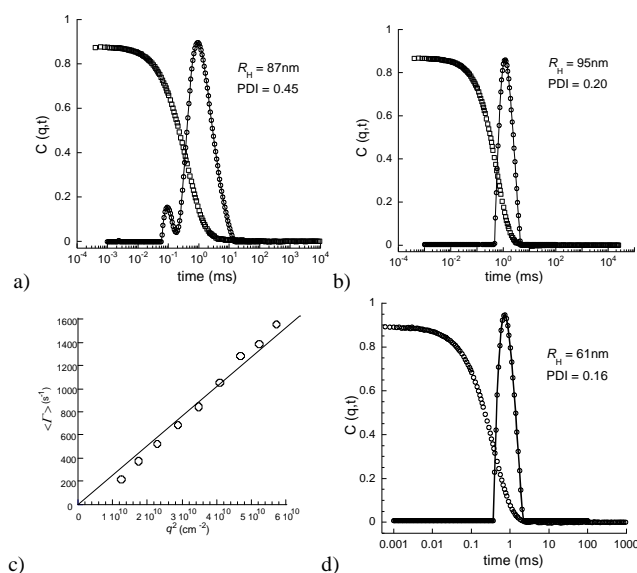


Fig. 2 DLS correlogram at a scattering angle of 90° and distribution of the correlation times for PDMAEMA₈₅-*b*-PBLG₄₁ nano-precipitated objects for a) water-to-THF injection; b) water-to-DMSO injection; c) multi-angle DLS illustrating the low PDI with water-to-DMSO injection by the perfect linearity of the mean decay rate $\langle \tau \rangle$ with the square of the scattering vector, q^2 ; d) DLS correlogram at 90° and distribution of the correlation times for hybrid objects made of PDMAEMA₈₅-*b*-PBLG₄₁ and γ -Fe₂O₃ USPIOs (10 wt. %) prepared by water-to-DMSO injection. The pH value was 6.5 for all the preparations.

In the case of water-to-THF injection (Fig. 2a), a bimodal distribution of relaxation times associated to large size dispersity was ascribed to the rather poor solubility of PBLG helices in THF.²⁵ Larger sizes were also found when this solvent was used to prepare PTMC-*b*-PGA polymersomes by nanoprecipitation.²⁶ On the contrary, water-to-DMSO injection leads to objects of same order of magnitude of size ($R_H=95$ nm) than direct dissolution, but with a much lower PDI=0.20 (Fig. 2b). The variation of the scattering angle of the goniometer between 50° and 130° led to a perfect linearity of the 1st order cumulant of the correlogram (z -average decay rate) vs. the square of the scattering vector (Fig. 2c), indicating the presence of isotropic scatterers with narrow size dispersity. To get an insight of the structure of the nanoparticles at a much lower scale, we used much higher

resolution techniques such as TEM (Fig. 3) and SANS (Fig. 4).

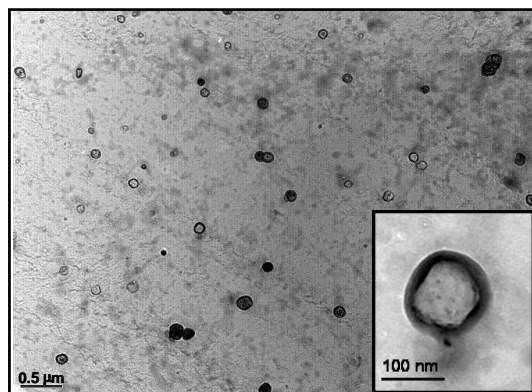


Fig. 3 TEM pictures of PDMAEMA₈₅-*b*-PBLG₄₁ vesicles prepared by water-to-DMSO nanoprecipitation at two magnifications (see scale bars).

The TEM pictures clearly showed hollow spheres with diameters ranging from 80 to 160 nm with an average around 120 nm. A close-up view at a larger magnification enabled to measure a membrane thickness of about 20±5nm.

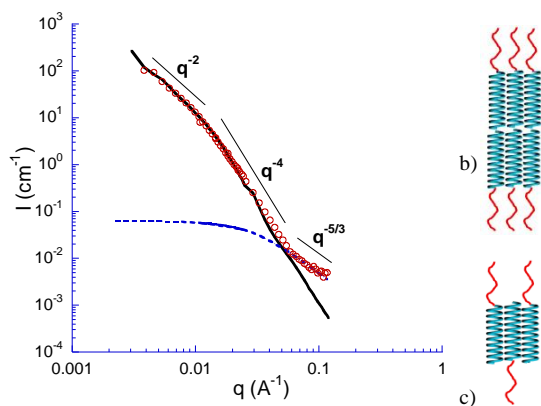


Fig. 4 a) SANS curve of PDMAEMA₈₅-*b*-PBLG₄₁ vesicles prepared by water-to-DMSO nanoprecipitation. In D₂O/DMSO-d₆, the scattering contrast comes from both polymer blocks. The solid curve represents the form factor of vesicles of median radius $R_0=90$ nm ($\sigma_{\text{radius}}=0.2$) and shell thickness $\delta_0=20$ nm ($\sigma_{\text{thickness}}=0.3$); b) Sketch for a PDMAEMA₈₅-*b*-PBLG₄₁ bilayer; c) Sketch of membrane in case of interdigitated helices.

The experimental SANS intensity exhibit several scaling law behaviours in the successive ranges of scattering vector. At low q , the intensity does not saturate because the gyration radius is too large to be accessible in the SANS q -range. In the intermediate q -regime, the intensity scaling law as q^{-2} is typical of flat membranes' structure of large vesicles. Then the Porod's regime varying like q^{-4} turns to $q^{-5/3}$ at high q presumably due to a rough interface of objects covered with Gaussian chains. The form factor of a shell of internal and external radii $R-\delta/2$ and $R+\delta/2$ was convolved with two Log-normal distributions of the radius and thickness (median values R_0 and δ_0 , widths σ_{radius} and $\sigma_{\text{thickness}}$) using appropriate averaging of polydispersity.²⁷ The median thickness $\delta_0=20$ nm of the fitted curve well compares to the TEM pictures. As described in the experimental part, the neutron SLD contrasts of PDMAEMA and PBLG with D₂O/DMSO-d₆ are comparable. Therefore the shell fit reflects the total thickness of the membrane. PBLG chains in helical conformation can be modelled by cylindrical rods of diameter

1.25 nm and of length 0.15 nm per γ -benzyl-L-glutamate monomer,²⁸ *i.e.* 6.15 nm for a degree of polymerization of 41. Thus we can imagine two extreme possibilities for the membrane formation with PDMAEMA₈₅-*b*-PBLG₄₁: either the copolymers form a bilayer with a hydrophobic thickness of 12 nm covered on both sides by a compact layer around 4 nm of hydrophilic coils (Fig. 4b), or the PBLG helices are interdigitated in a narrower layer about 6 nm enabling the hydrophilic chains to be in a much more stretched conformation around 7 nm (Fig. 4c). The latter situation is likely in better agreement with the vesicle geometry for the charged PDMAEMA chains in a brush regime due to confinement at a locally planar interface

C. Hybrid self-assembled structures

Compared to previous case of “blank” pure copolymer particles, the DLS results for hybrids at 10 wt. % shown in Fig. 2d were rather striking due to a lower hydrodynamic size ($R_H=61$ nm) and a narrower size distribution (PDI=0.16). This result was supported by observation of the TEM images, showing much more compact objects (Fig. 5 vs. Fig. 3). However, one should be aware of artefacts due to the projection effect of TEM onto a planar surface and to the lower electron scattering density of the copolymer compared to γ -Fe₂O₃. Therefore SANS measurements were also necessary to decipher the exact arrangement of USPIOs within the hybrid particles.

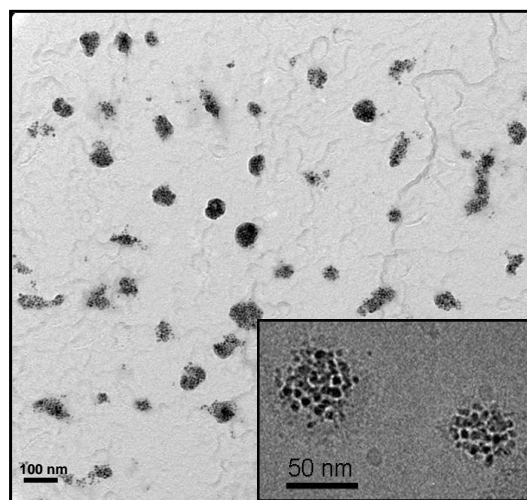


Fig. 5 TEM pictures of PDMAEMA₈₅-*b*-PBLG₄₁ / γ -Fe₂O₃ (10 wt. %) hybrid nanoparticles prepared by water-to-DMSO injection at two magnifications (see scale bars).

Unlike previous SANS measurements with pure copolymer particles in deuterated solvents mixture, the solvent used for hybrid particles was light water in order to benefit from the large neutron SLD contrast of iron oxide relatively to H₂O (see part 2. D. Methods). A centrifugation step was also applied to increase the concentration and thus the SANS intensity. For two weight ratios of γ -Fe₂O₃ to copolymer, the curves plotted on Fig. 6 were well adjusted by the form factor of filled polydisperse spheres of radii with a Log-normal distribution law of median $R_0=18$ nm and width $\sigma=0.25$. The scaling law as q^{-2} typical of the membrane of large vesicles was clearly not observed here, attesting a structural change when the copolymer was self-assembled in the presence of the inorganic nanoparticles with a hydrophobic coating. While

inaccessible by SANS for the pure copolymer vesicles, the radius of gyration measured by Guinier's plots was 19.9 and 19.2 nm respectively for 10 and 20 wt. % hybrids.

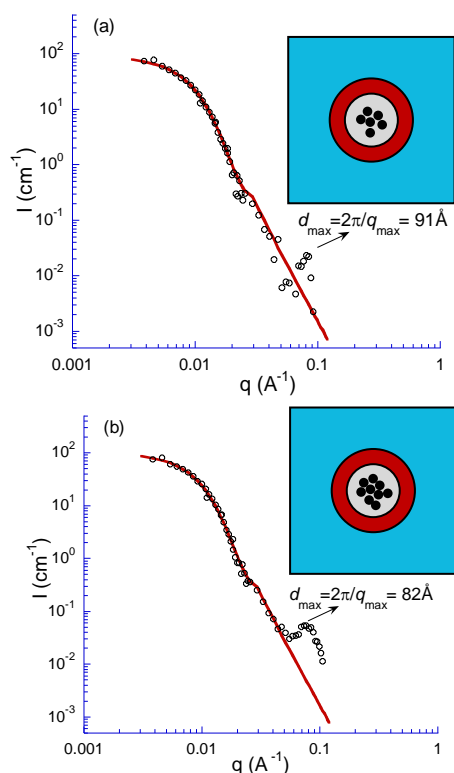


Fig. 6 SANS curve of PDMAEMA₈₅-*b*-PBLG₄₁ / γ -Fe₂O₃ hybrid particles prepared by water-to-DMSO injection at (a) 10 and (b) 20 wt. %. In both cases, the solid curve represents the form factor of polydisperse filled spheres with a Log-normal distribution law of radii of median $R_0=18$ nm and width $\sigma=0.25$. The sketches in insets represent the nanoscale structure of core-shell micelles with the USPIOs (in black) closely packed in PBLG hydrophobic cores (in grey) wrapped by a hydrated PDMAEMA shell not contributing to the SANS contrast in H₂O (in red).

In addition, the curves clearly displayed a structure peak at large q values. Its maximum was measured at q_{\max} around 0.069 \AA^{-1} for 10 wt. % and 0.076 \AA^{-1} for 20 wt. %, corresponding to a strong correlation of centre-to-centre distances $d_{\max}=2\pi/q_{\max}$ around 9.1 and 8.2 nm respectively. Considering the sizes of the γ -Fe₂O₃ cores (Log-normal law of $d_0=6.3$ nm and width $\sigma=0.22$), these USPIOs were closely packed inside the objects as observed on Fig. 5 and sketched in the insets of Fig. 6. More precisely, we can calculate that inside the objects, USPIOs have a local volume fraction $\Phi_{\text{local}} = \pi/6(d_w/d_{\max})^3$ where d_w is the weight averaged diameter of the Log-normal law, given by $d_w = d_0 \exp(7\sigma^2/2)$. Numerically, we found $d_w=7.5$ nm, $\Phi_{\text{local}}=29\%$ for 10 wt. % and $\Phi_{\text{local}}=40\%$ for 20 wt. %. These values are much higher than the average volume fractions if the USPIOs were homogeneously distributed in the hydrophobic part of the hybrids: from the mass density of PBLG (1.44 g/cm³) and γ -Fe₂O₃ (5.1 g/cm³) and the weight fraction of PBLG (60%) in PDMAEMA₈₅-*b*-PBLG₄₁, we calculate $\Phi_{\text{ave}}=5\%$ for 10 wt. % and $\Phi_{\text{ave}}=10.5\%$ for 20 wt. %. Another calculation aims at estimating the number of USPIOs per object in each case according to $N_{\text{USPIO}} = \Phi_{\text{local}}(d_{\text{core}}/d_w)^3$, where d_{core} stands for the diameter of hydrophobic core sketched in grey on Fig. 6. As only γ -Fe₂O₃ and PBLG contribute to the

neutron SLD contrast (but not the hydrated shell of PDMAEMA), we calculate a core size $d_{\text{core}} = 2R_0 \exp(7\sigma^2/2) = 44.8$ nm using $R_0=18$ nm and $\sigma=0.25$ as used to fit the SANS curves. Therefore the estimates of average numbers of clustered USPIOs are $N_{\text{USPIO}}=62$ for 10 wt. % and $N_{\text{USPIO}}=85$ for 20 wt. %.

4. Discussion

Thermally induced morphology transition from micelles to vesicles has been recently described for a diblock copolymer.²⁹ A bilayer-to-micelle transition by incorporation of USIPOs has been recently described with a PS-*b*-PAA diblock copolymer.¹⁵ In the latter case, the volume fraction at the onset of the transition was located around 12%, whereas the fraction of micelles progressively increased for larger Φ . However, true magnetopolymerosomes could be obtained with up to 35.8 wt. % of oleic acid coated magnetite USPIOs in PS-*b*-PAA. For PI-*b*-PEO, a phenomenon of bilayer bridging by the USPIOs was observed when the weight ratio of iron oxide exceeded 20 – 30 wt. %.¹⁴ Nevertheless, the stable structure still consisted in polymer vesicles, in spite of their multi-lamellar structure. In the case of PTMC-*b*-PGA, magnetic membranes were observed up to 70 wt. %, while the limit was pushed further than twice the polymer content with a soft elastomeric hydrophobic block such as in PB-*b*-PGA.¹³ On the contrary, this study shows that the PDMAEMA₈₅-*b*-PBLG₄₁ vesicle self-assembling structure cannot even withstand to a volume fraction as low as $\Phi_{\text{ave}}=5\%$ of USPIOs in the PBLG blocks. This phenomenon is reminiscent of the phase behaviour of USPIOs of same sizes, nature and surfactant coating in the nematic thermotropic liquid crystal 4-pentyl-4'-cyanobiphenyl:²⁰ while the inorganic nanoparticles are properly dispersed in the isotropic phase (up to $\Phi = 0.83\%$ at least), they are expelled towards the defect lines as soon as temperature is lowered below the nematic-to-isotropic transition, even at a fraction as small as $\Phi = 0.08\%$. This analogy is worth mentioning since PBLG is known itself to exhibit lyotropic liquid crystal phases²⁸ and to have a rod-like conformation in such solvents.³⁰ Thus in the following, we present a discussion in the framework of the complex phase behaviour of binary mixtures of spherical and rod-like particles driven by the depletion interaction.³¹

Entropic in nature, this interaction originates from osmotic pressure forces acting on hard spheres immersed in a suspension of cylindrical rods, the volume excluded to rods being described by a depletion layer surrounding the spheres. Referring to a model in the literature,³² we calculate the attractive depletion potential acting between two hard spheres with their surfaces at a distance H : $U_{\text{depl}}(H)/k_B T = \Phi_{\text{rods}}(LR/D^2)K_1(H/L)$. Here the α -helices of PBLG are modelled as rigid cylinders of length $L=6.15$ nm and diameter $D=1.25$ nm, thus of aspect ratio $L/D \approx 5$. The USPIOs are quasi-spherical nanoparticles with a typical radius $R=d_w/2=3.75$ nm. The binary mixture is thus characterized by a size ratio of rod length to sphere radius $L/R \approx 1.64$. The value of the potential when the spheres are at close contact ($H=0$) is given by the value of the function $K_1(0)$ calculated numerically in this reference and leading to $K_1(0)=-0.219$.[‡] Using $LR/D^2 \approx 14.8$ in the present geometry and $\Phi_{\text{rods}}=1-\Phi_{\text{ave}}$ in the hydrophobic cores, we calculate $U_{\text{depl}}(H=0)/k_B T \approx -3.1$ and -2.9 respectively for 10 and 20 wt. % of USPIOs in the copolymer. Therefore the depletion

attraction between USPIOs is large enough to compete with thermal agitation energy and induce a phase separation between the quasi-spherical $\gamma\text{-Fe}_2\text{O}_3$ nanoparticles and the rod-like blocks of the copolymer. The same model can predict the maximum size of spheres embedded in PBLG helical blocks that would not lead

to phase separation, due to $U_{\text{depl}}(H=0) < k_B T$: we find $R_{\text{max}} = 2$ nm. Although this lower size would significantly decrease the properties of the USPIOs for MRI, it would be still interesting to use them in hybrids as T_1 contrasting agents instead of T_2 .³³

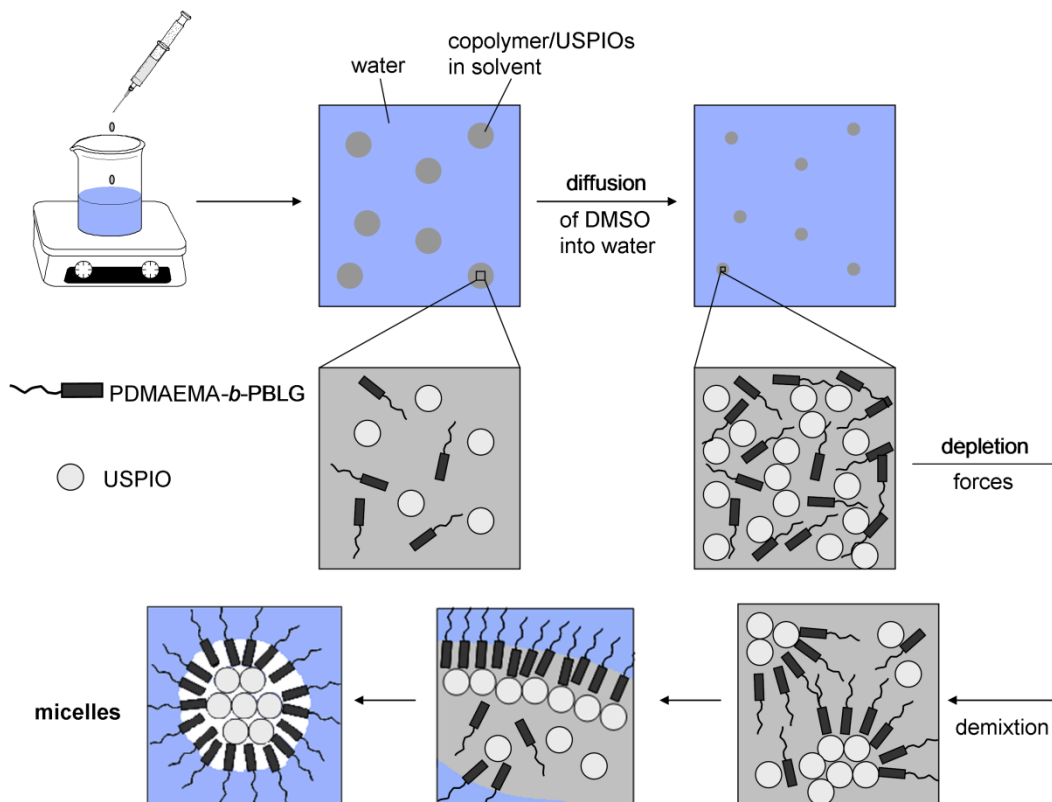


Fig. 7 Sketch of the micro-phase separation due to depletion attraction between USPIO spheres in PBLG rods leading to the vesicle-to-micelle transition.

The successive steps of the self-assembly of hydrophobically coated USPIOs and PDMAEMA₈₅-*b*-PBLG₄₁ is sketched on Fig. 7. When water is slowly added in the DMSO solution containing both the rod-coil copolymer and the quasi-spherical magnetic nanoparticles, the solvent quality decreases progressively for PBLG and the hydrophobically coated $\gamma\text{-Fe}_2\text{O}_3$ nanoparticles that concentrate in DMSO rich domains, increasing their local concentration. At some point, when the solvent mixture becomes really poor, the system “precipitates” at a nanometric scale, leading to very high concentrations of the components locally. The depletion forces between $\gamma\text{-Fe}_2\text{O}_3$ spheres in PBLG rods are then so large within the hydrophobic cores that the binary system demixes into internal domains. To explain the transition between the demixed droplet and the final cartoon, we invoke the spontaneous curvature of the USPIO favouring a core-shell micelle with the close-packed nanospheres in the core and expelling the rod-like copolymer at the interface with the hydrophilic shell.

Conclusions

Colloidal suspensions are present in many synthetic materials, such as paints, glues, inks, and in biological components like cells, bacteria and viruses. In living systems, they exhibit important transport and structural properties that mainly depend

on the size, shape, concentration and composition. Depletion forces are playing an important role in the equilibrium phases of such complex systems, with an important contribution of the excluded-volume interaction to the free energy. We have demonstrated here that the self-assembled structure of rod-coil amphiphilic diblock copolymers mixed with quasi-spherical nanoparticles is not only governed by their amphiphilic character, but also by excluded-volume interactions. This experimental demonstration opens an interesting route for the design of complex and controlled assemblies of hybrid nanostructures using depletion effects combined to self-assembly. It is known that such entropic effects can produce crystal arrays of colloids,³⁴ but also affect the function of a cell.³⁵ This means that such forces are not only playing an important role in the structural and physical properties of such systems, but also in their functions.

Notes and references

^a Université de Bordeaux/IPB, ENSCBP, 16 avenue Pey Berland, 33607 Pessac Cedex, France.

^b CNRS, Laboratoire de Chimie des Polymères Organiques (UMR5629), Pessac, France.

^c CEA Saclay, LLB, 91191 Gif sur Yvette, France

^d CNRS, Laboratoire Léon Brillouin (UMR12), Gif sur Yvette, France

*Correspondence to SL: E-mail: lecommandoux@enscbp.fr; Fax: +33 5 4000 8487; Tel: +3 5 4000 2241; and OS: E-mail: osandre@enscbp.fr; Fax: +33 5 4000 8487; Tel: +3 5 4000 3695;

† Electronic Supplementary Information (ESI) available: Fig. S1 Magnetization curve vs. applied magnetic field and distribution law of diameters for the USPIOs dispersed in CH₂Cl₂. Fig. S2 DSC curves representing the heat flow (mW/g) vs. temperature (°C) for the copolymer and the homopolymers. See DOI: 10.1039/C1SM05638G

$$K_1(0) = -\pi/6(1 + 0.8762L/R)/(1 + 1.33198L/R + 0.98225(L/R)^2)$$

10

- 1 I. W. Hamley and V. Castelletto, *Angew. Chem. Int. Ed.* 2007, **46**, 4442.
- 2 R. J. Ellis, *Trends in Biochem. Sciences* 2001, **26**, 597; A.P. Minton, *J. Biol. Chem.* 2001, **276**, 597; R. J. Ellis, *Nature* 2002, **416**, 483; M. Kinoshita and T. Oguni, *Chem. Phys. Lett.* 2002, **351**, 79
- 3 B. Götzelmann, R. Roth, S. Dietrich, M. Dijkstra and R. Evans, *Europhys. Lett.* 1999, **47**, 398 ; R. Roth, R. Evans and S. Dietrich, *Phys. Rev. E* 2000, **62**, 5360.
- 4 D. Rudhardt, C. Bechinger and P. Leiderer, *Phys. Rev. Lett.* 1998, **81**, 1330 ; R. Verma, J. C. Crocker, T.C. Lubensky and A.G. Yodh, *Phys. Rev. Lett.* 1998, **81**, 4004.
- 5 H. Bermudez, A. K. Brannan, D.A. Hammer, F. S. Bates and D. E. Discher, *Macromolecules* 2002, **35**, 8203.
- 6 W. Agut, A. Brûlet, C. Schatz, D. Taton and S. Lecommandoux, *Langmuir* 2010, **26**, 10546.
- 7 H. Schlaad, *Adv. Polym. Sci.* 2006, **202**, 53; J. Rodriguez-Hernandez, S. Lecommandoux, *J. Am. Chem. Soc.* 2005, **127**, 2026; E. P. Holowka, D. J. Pochan and T. J. Deming, *J. Am. Chem. Soc.* 2005, **127**, 12423; E. G. Bellomo, M. D. Wyrsta, L. Pakstis, D. J. Pochan and T. J. Deming, *Nat Mater* 2004, **3**, 244; A. Carlsen and S. Lecommandoux, *Curr. Opin. Colloid Interface Sci.* 2009, **14**, 329.
- 8 S. Mornet, S. Vasseur, F. Grasset and E. Duguet, *J. Mat. Chem.* 2004, **14**, 2161.
- 9 R. Weissleder, D. Stark, B. L. Engelstad, B. R. Bacon, C. C. Compton, D. L. White, P. Jacobs and J. Lewis, *Am. J. Roentgenol.* 1989, **152**, 167.
- 10 H. Ai, C. Flask, B. Weinberg, X. T. Shuai, M. D. Pagel, D. Farrell, J. Duerk, J. Gao, *Adv. Mat.* 2005, **17**, 1949; B.-S. Kim, J.-M. Qiu, J.-P. Wang and T. A. Taton, *Nano Lett.* 2005, **5**, 1987.
- 11 J.-F. Berret, N. Schonbeck, F. Gazeau, D. El Kharrat, O. Sandre, A. Vacher and M. Airiau, *J. Am. Chem. Soc.* 2006, **128**, 1755
- 12 C. Paquet, H. W. de Haan, D. M. Leek, H.-Y. Lin, B. Xiang, G. Tian, A. Kell and B. Simard, *ACS Nano* 2011, **5**, doi: 10.1021/nn2002272.
- 13 S. Lecommandoux, O. Sandre, F. Chécot, J. Rodriguez-Hernandez, and R. Perzynski, *Adv. Mat* 2005, **17**, 712; S. Lecommandoux, O. Sandre, F. Chécot, J. Rodriguez-Hernandez and R. Perzynski, *J. Magn. Magn. Mater.* 2006, **300**, 71; S. Lecommandoux, O. Sandre, F. Chécot and R. Perzynski, *Progr. Sol. State Chem.* 2006, **34**, 171.
- 14 M. Krack, H. Hohenberg, A. Kornowski, P. Lindner, H. Weller and S. Förster, *J. Am. Chem. Soc.* 2008, **130**, 7315.
- 15 R. J. Hickey, B. L. Sanchez-Gaytan, W. Cui, R. J. Composto, M. Fryd, B. B. Wayland and S.-J. Park, *Small* 2009, **6**, 48; R. J. Hickey, A. S. Haynes, J. M. Kikkawa and S.-J. Park, *J. Am. Chem. Soc.* 2010, **133**, 1517.
- 16 C. Sanson, O. Diou, J. Thévenot, E. Ibarboure, A. Soum, A. Brûlet, V. Dupuis, S. Miraux, E. Thiaudière, S. Tan, A. Brisson, O. Sandre and S. Lecommandoux, *ACS Nano* 2011, **5**, 1122.
- 17 W. Agut, D. Taton and S. Lecommandoux, *Macromolecules*, 2007, **40**, 5653.
- 18 R. Massart, *IEEE Trans. on Magnetics* 1981, **MAG-17**, 1247.
- 19 R. Massart, E. Dubois, V. Cabuil, E. Hasmonay, *J. Mag. Mag. Mat.*, 1995, **149**, 1.
- 20 C. Da Cruz, O. Sandre, V. Cabuil, *J. Phys. Chem. B* 2005, **109**, 14292.
- 21 C. Allen, D. Maysinger and A. Eisenberg, *Colloids and Surf. B: Biointerfaces*, 1999, **16**, 3.
- 22 M. E. Yildiz, R. K. Prud'homme, I. Robb and D. H. Adamson, *Polym. Adv. Technol.*, 2007, **18**, 427.
- 23 J.-P. Cotton in *Neutron, X-Ray and Light Scattering*, P. Lindner, T. Zemb Ed., Elsevier, North-Holland, Delta series, 1991, chap. II, p.19.
- 24 H.-A. Klok, J. F. Langenwalter and S. Lecommandoux, *Macromolecules* 2000, **33**, 7819; S. Lecommandoux, M.-F. Achard, J. F. Langenwalter and H.-A. Klok, *Macromolecules* 2001, **34**, 9100.
- 25 F. Sanda, G. Gao and T. Masuda, *Macromol. Bioscience* 2004, **4**, 570.
- 26 C. Sanson, C. Schatz, J.-F. Le Meins, A. Brûlet, A. Soum and S. Lecommandoux, *Langmuir* 2010, **26**, 2751.
- 27 J. S. Pedersen, *Adv. in Coll. and Interf. Sci.* 1997, **70**, 171.
- 28 S. M. Yu, V. P. Conticello, G. Zhang, C. Kayser, M. J. Fournier, T. L. Mason and D. A. Tirrell, *Nature*, 1997, **389**, 167.
- 29 A. O. Moughton and R. K. O'Reilly, *Chem. Commun.* 2010, **46**, 1091.
- 30 J. S. Crespo, S. Lecommandoux, R. Borsali, H.-A. Klok and V. Soldi, *Macromolecules* 2003, **36**, 1253.
- 31 M. Adams, Z. Dogic, S. L. Keller and S. Fraden, *Nature*, 1997, **393**, 349; G.A. Vliegthart and H.N.W. Lekkerkerker, *J. Chem. Phys.* 1999, **111**, 4153.
- 32 K. Yaman, C. Jeppesen and C. M. Marques, *Europhys. Lett.*, 1998, **42**, 221.
- 33 U. I. Tromsdorf, O. T. Bruns, S. C. Salmen, U. Beisiegel and H. Weller, *Nano Lett.* 2009, **9**, 4434.
- 34 A. D. Dinsmore and A. G. Yodh, *Langmuir* 1998, **15**, 314.
- 35 R. Roth, B. Götzelmann and S. Dietrich, *Phys. Rev. Lett.* 1999, **83**, 448.